INVESTIGATION OF THE MILLER CYCLE ON THE PERFORMANCE AND EMISSION IN A NATURAL GAS-DIESEL DUAL-FUEL MARINE ENGINE BY USING TWO ZONE COMBUSTION MODEL

by

***Huibing GAN* *, Huaiyu WANG, YuanYuan TANG, and GuanJie WANG**

Marine Engineering College, Dalian Maritime University, Dalian, China

Original scientific paper
https://doi.org/10.2298/TSCI190518420G

Compared to the standard cycle, the Miller cycle decreases the cylinder maximum combustion temperature which can effectively reduce NO_x emissions. In this paper, a 0-D two-zone combustion model is used to establish the simulation model of a marine dual-fuel engine, which is calibrated according to the test report under different loads. Due to the high emissions under part load, the Miller cycle (early intake valve closing method) is used for optimization. By analyzing the cylinder pressure, temperature, heat release rate, and NO_x emissions under different cases, it can be found that the effective working volume and thermal efficiency decrease with the advance of intake valve closing and improve with the increase of the geometric compression ratio. In all optimization cases, the NO_x emissions and fuel consumption are reduced by 72% and 0.1%, respectively, by increasing the geometric compression ratio to 14 and the intake valve closing timing to 510 °CA (the reference top dead center is 360 °CA). The simulation results show that the early intake valve closing Miller cycle can effectively reduce the NO_x emissions and cylinder peak pressure.

Key words: *Miller cycle, dual-fuel engine, 0-D two-zone combustion model, reduce NO_x emission, geometric compression ratio*

Introduction

With the implementation of IMO Tier III emission requirements, more stringent requirements are imposed on the marine engines NO_x emissions [1]. Current technologies for reducing NO_x emissions mainly include exhaust gas re-circulation (EGR) [2], exhaust gas selective catalytic reduction [3], electronically controlled fuel injection technology [4], Miller cycle [5] and so on. In addition, natural gas-diesel dual-fuel engines are considered to be a more attractive solution due to higher natural gas reserves and lower emissions [6-8]. Combined with the Miller cycle, NO_x emission in dual-fuel engine can be further reduced [9, 10]. The Miller cycle reduces the effective working volume of the cylinder by changing the intake valve closing timing such that the effective compression ratio is less than the expansion ratio. The Miller cycle reduces the maximum cylinder combustion temperature and thus reduces emissions [11]. Wang *et al.* [12] used the late intake valve closing to achieve the Miller cycle in reducing gasoline engine emissions. The characteristics of the Otto cycle and the Miller cycle were compared. The results show that the Miller cycle reduces NO_x emissions by reducing the in-cylinder combustion temperature. Mikalsen *et al.* [13] studied the feasibility of a small

* Corresponding author, e-mail: ghbzq@dlmu.edu.cn

natural gas engine for cogeneration applications, and the Miller cycle can improve fuel efficiency [13]. Gonca and Sahin [14] used the Miller cycle and intake humidification method on a supercharged Diesel engine. The experimental results show that the Miller cycle combined with intake humidification can effectively reduce NO_x emissions and it is better than use the Miller cycle alone. Tavakoli *et al.* [15] applied the Miller cycle to a lean-burn natural gas engine and analyzed the performance and emission characteristics of a four-stroke supercharged gas engine using a finite volume method. The results show that the late intake valve closing improves engine performance, but the peak pressure and temperature variation in the cylinder is not significant. Yan *et al.* [16] studied Miller's optimization of the combustion and performance of a stoichiometric natural gas engine. Through thermodynamic analysis, as the geometric compression ratio increases, the potential for higher thermal efficiency increases. Kayadelen *et al.* [17] and Gonca *et al.* [18] used a two-zone combustion model to apply the Miller cycle to a Diesel engine and compared it to a conventional Diesel engine. The 0-D two-zone combustion has the advantages of simple model modeling and fast calculation speed. It is not inferior to the quasi-dimensional or 3-D model in the optimization and improvement of the internal combustion engine [19]. Since there is no variable valve timing system in the original engine, the purpose of this paper is to discuss the feasibility of Miller cycle application in marine low-speed engines. The model is built by a 0-D two-zone combustion model, and the Miller cycle is achieved by the early intake valve closing method. The optimal operating point for engine emissions and performance at low loads was investigated by Miller cycle and varying geometric compression ratios. This paper explores the feasibility of applying the Miller cycle for the dual-fuel engine and provides a reasonable solution for the marine medium-speed engine to reduce emissions at part load and meet the Tier III standard.

Miller cycle principle and modeling theory

Miller cycle principle

The effective compression ratio of the Miller cycle intake stroke is less than the expansion ratio of the exhaust stroke compared to the standard cycle. There are three ways to achieve the Miller cycle: Install a rotary valve between the intake manifold and the intake valve to control the amount of intake air. This is the so-called intake control rotary valve (ICRV) [20]; The intake valve is closed before the end of the intake stroke, *i. e.* the early intake valve closing (EIVC) [21] and; Keep the intake valve open during a portion of the compression stroke to exclude some of the gas and reduce the effective compression ratio, *i. e.* the late intake valve closing (LIVC) [16, 22].

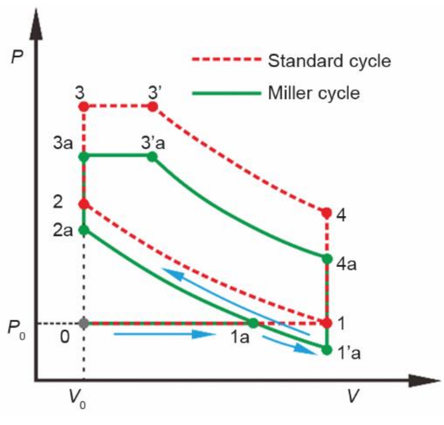

Figure 1. Comparison of standard and Miller cycles

Figure 1 shows a comparison of the EIVC Miller cycle and the standard cycle [23]. The diesel engine standard cycle curve is 0-1-2-3-3'-4-1-0. The workflow is: 1 – the intake stroke is 0-1, and when the piston moves to BDC, the intake valve closes. 2 – Compression stroke is 1-2. 3 – Combustion and expansion stroke is 2-3-3'-4. 4 – exhaust stroke is 4-1-0. The Miller cycle curve is 0-1a-1'a-2a-3a-3'a-4a-1-0. The workflow is: 1 – the intake stroke is 0-1a, and when the piston moves to 1a, the intake valve closes and the piston still moves down from 1a to 1'a. Since the intake valve is closed, the air in the cylinder is lowered due to expansion, and the temperature is lower than the standard cycle. 2 – Compression stroke is 1'a-2a. The cylinder pressure at the end of compression is lower than the standard cycle, and the air temperature in the cylinder is also lower than the standard cycle. 3 – Combustion and expansion stroke is 2a-3a-3'a-4a. Its highest cylinder pressure is lower than the standard cycle, and the maximum combustion temperature in the cylinder is also lower than the standard cycle. 4 – Exhaust stroke is 4a-1-0. Compared with the standard cycle, the Miller cycle reduces the maximum combustion temperature in the cylinder, so that the NO_x generation region is avoided during the combustion process to achieve the purpose of reducing NO_x.

Modeling theory

In this paper, the 0-D two-zone combustion model is used to calculate emissions and performance [19]. The cylinder is divided into a burned zone and an unburned zone at the start of injection. The fuel in the unburned zone reacts with the air to become part of the burned zone. The energy conservation equation in the cylinder can be expressed:

$$\frac{\mathrm{d}U}{\mathrm{d}\phi}=\frac{\mathrm{d}(mu)}{\mathrm{d}\phi}=\frac{\mathrm{d}Q_\mathrm{f}}{\mathrm{d}\phi}+h_\mathrm{s}\frac{\mathrm{d}m_\mathrm{s}}{\mathrm{d}\phi}-h_\mathrm{e}\frac{\mathrm{d}m_\mathrm{e}}{\mathrm{d}\phi}-\frac{\mathrm{d}Q_\mathrm{w}}{\mathrm{d}\phi}-p\frac{\mathrm{d}V}{\mathrm{d}\phi} \tag{1}$$

where u is specific internal energy and the temperature changes in the cylinder is:

$$\frac{\mathrm{d}T}{\mathrm{d}\phi}=\frac{1}{mc_\mathrm{v}}\left(\frac{\mathrm{d}Q_\mathrm{f}}{\mathrm{d}\phi}+h_\mathrm{s}\frac{\mathrm{d}m_\mathrm{s}}{\mathrm{d}\phi}-h_\mathrm{e}\frac{\mathrm{d}m_\mathrm{e}}{\mathrm{d}\phi}-\frac{\mathrm{d}Q_\mathrm{w}}{\mathrm{d}\phi}-p\frac{\mathrm{d}V_\mathrm{b}}{\mathrm{d}\phi}-u\frac{\mathrm{d}m}{\mathrm{d}\phi}\right) \tag{2}$$

Ignore valve leakage and by-pass flow, assuming the total mass in the cylinder is constant, the total mass of the burned zone and the unburned zone is:

$$m=m_\mathrm{u}+m_\mathrm{b} \tag{3}$$

The total volume of the burned zone and the unburned zone is equal to the total volume of the cylinder:

$$V=V_\mathrm{u}+V_\mathrm{b} \tag{4}$$

The research engine's piston pin in this paper has no offset, so the total cylinder volume function is:

$$\frac{\mathrm{d}V}{\mathrm{d}\phi}=\frac{\mathrm{d}\pi}{8}B^2S\sin\phi\left[1+\varepsilon\frac{\cos\phi}{\sqrt{(1-\varepsilon^2\sin^2\phi)}}\right] \tag{5}$$

In each region, assuming the ideal gas and the same pressure, the equation of state are:

$$\begin{cases}pV_\mathrm{u}=m_\mathrm{u}\mathrm{R}_\mathrm{u}T_\mathrm{u}\\ pV_\mathrm{b}=m_\mathrm{b}\mathrm{R}_\mathrm{b}T_\mathrm{b}\end{cases} \tag{6}$$

where the R_u and R_b are the gas constant of unburned and burned zone.

The energy equations for each region are [24]:

$$\begin{cases} \dfrac{\mathrm{d}(m_\mathrm{u}u_\mathrm{u})}{\mathrm{d}\phi} = -p\dfrac{\mathrm{d}V_\mathrm{u}}{\mathrm{d}\phi} + \dfrac{\mathrm{d}Q_\mathrm{w,u}}{\mathrm{d}\phi} - h_\mathrm{u}\dfrac{\mathrm{d}m_\mathrm{u}}{\mathrm{d}\phi} \\ \dfrac{\mathrm{d}(m_\mathrm{b}u_\mathrm{b})}{\mathrm{d}\phi} = -p\dfrac{\mathrm{d}V_\mathrm{b}}{\mathrm{d}\phi} + \dfrac{\mathrm{d}Q_\mathrm{w,b}}{\mathrm{d}\phi} + h_\mathrm{u}\dfrac{\mathrm{d}m_\mathrm{u}}{\mathrm{d}\phi} \end{cases} \tag{7}$$

The Wiebe function is used to describe the heat release rate [25]:

$$\frac{\mathrm{d}x}{\mathrm{d}\phi} = a\frac{m+1}{\phi_\mathrm{b}}\left(\frac{\phi-\phi_0}{\phi_\mathrm{b}}\right)^m \exp\left[-a\left(\frac{\phi-\phi_0}{\phi_\mathrm{b}}\right)^{m+1}\right] \tag{8}$$

where the m is the combustion shape factor, a – the Wiebe constant, and 6.908 for complete combustion.

For the combustion duration and ignition delay, id, at variable working condition [26]:

$$\phi_\mathrm{b} = \phi_\mathrm{b,ref}\left(\frac{s_\mathrm{ref}}{s}\right)^{2/3}\left(\frac{n}{n_\mathrm{ref}}\frac{f_\mathrm{ref}}{f}\right)^{1/3} \tag{9}$$

$$id = id_\mathrm{ref}\left(\frac{s_\mathrm{ref}}{s}\frac{f}{f_\mathrm{ref}}\right)^{2/3}\left(\frac{n}{n_\mathrm{ref}}\right)^{1/3} \tag{10}$$

where s, id, and f mean laminar flame speed, ignition delay, and piston to head distance at ignition timing, respectively. The laminar flame velocity is a function of in-cylinder conditions, air-fuel ratio, and residual gas mole fraction and it is obtained by looking up the table [27].

The natural gas is mixed with air at the intake port and the diesel directly injected into the cylinder. It is assumed that the diesel fuel is instantaneously atomized and uniformly mixed in the cylinder, and the formed mixture is evenly distributed in the cylinder. The injected diesel fuel evaporates immediately and there is no liquid fuel zone in the cylinder. The chemical reaction equation is simplified to:

$$\mathrm{C}_x\mathrm{H}_y\mathrm{O}_z + \left(x+\frac{y}{4}-\frac{z}{2}\right)\left(\mathrm{O}_2+\frac{79}{21}\mathrm{N}_2\right) \to x\mathrm{CO}_2 + \frac{y}{2}\mathrm{H}_2\mathrm{O} + \frac{79}{21}\left(x+\frac{y}{4}-\frac{z}{2}\right)\mathrm{N}_2 \tag{11}$$

The heat release of diesel accounts for less than 2% of the total heat release, so the mass-flow of diesel is converted to natural gas mass according to the heat release of diesel.

For the species thermodynamic parameters, the working gas in the cylinder is assumed to be ideal gas and the single gas parameters is [28]:

$$c_\mathrm{p} = a_1 + a_2\theta + a_3\theta^2 + \cdots\cdots + a_k\theta^{k-1}\cdots\cdots a_m\theta^m \tag{12}$$

$$\theta = \frac{(T - T_\mathrm{shift})}{T_\mathrm{norm}}$$

where a_i and θ are the fitting coefficient of constant pressure specific heat and normalized temperature, respectively. The typical values of T_shift and T_norm are 0 K and 1000 K, respectively [29].

Heat transfer is ongoing at all stages of the engine. It is generally believed that the combustion phase is dominated by intense radiation, while the other phases are dominated by convection and heat conduction. The Newton formula is used to describe the heat transfer model in the 0-D model [30]:

$$\frac{\mathrm{d}Q_\mathrm{w}}{\mathrm{d}\phi}=\sum_{i=1}^{3}\alpha_\mathrm{w}A_\mathrm{i}(T_z-T_\mathrm{wi}) \tag{13}$$

The Woschni [31] heat transfer model converts complex heat dissipation calculations into heat transfer coefficient calculations:

$$\alpha_\mathrm{w}=C_0D^{-0.2}p^{0.8}T^{-0.53}\left[C_1C_\mathrm{m}+C_2\cdot\frac{V_DT_1}{P_1V_1}(p-p_\mathrm{mot})\right]^{0.8} \tag{14}$$

For the part load:

$$\begin{cases}\alpha_\mathrm{w}=C_0D^{-0.2}p^{0.8}T^{-0.53}(C_1C_m+I)^{0.8}\\ I=\max\left[C_2\dfrac{V_DT_1}{P_1V_1}(p-p_\mathrm{mot}),2C_1C_m\left(\dfrac{V_C}{V}\right)^2\mathrm{IMEP}^{-0.2}\right]\end{cases} \tag{15}$$

Table 1 shows the coefficient C_1 and C_2 [24].

Table 1. Coefficients C_1 and C_2 for Woschni's correlation

Phase	C_1 [–]	C_2 [ms^{-1}K]
Intake-exhaust	6.18	0
Compression	2.28	0
Combustion-expansion	2.28	3.24×10^{-3}

When the turbocharger works in a stable condition, the compressor power consumption is theoretically equal to the available output power of the turbine. To simplify the model, the total mechanical losses are borne by the exhaust turbine. The exhaust turbine output power is:

$$\dot{W}_\mathrm{t}=\dot{m}_\mathrm{t}c_\mathrm{p}T_\mathrm{e}\eta_\mathrm{t}(1-w_\mathrm{t}^{\gamma}) \tag{16}$$

The input power of the compressor is:

$$\dot{W}_\mathrm{c}=\dot{m}_\mathrm{c}c_\mathrm{p}T_\mathrm{a}\frac{1}{\eta_\mathrm{c}}(w_\mathrm{c}^{\gamma}-1) \tag{17}$$

The compressor outlet temperature is:

$$T_\mathrm{c}=T_\mathrm{a}\left[1+\frac{1}{\eta_\mathrm{c}}(w_\mathrm{c}^{\gamma}-1)\right] \tag{18}$$

The turbocharger outlet temperature is very high and requires an intercooler for cooling. The intercooler can be simplified to the throttling process, the intercooler outlet temperature is:

$$T_\mathrm{i}=T_\mathrm{c}-\eta_s(T_\mathrm{c}-T_\mathrm{wi}) \tag{19}$$

In general, NO in Diesel engine emissions is derived from the reaction of nitrogen and oxygen at high temperature. According to the extended Zeldovich mechanism [32], the three-step NO formation reaction is as follows, and the reaction constants are shown in tab. 2.

$$k = A_\mathrm{A} T^{B_\mathrm{A}} \mathrm{e}^{\frac{E_\mathrm{A}}{T}} \tag{20}$$

Table 2. Reactions of NO formation

No. reaction		Forward/backward		
		A_A [cm^3 mol^{-1}s^{-1}]	B_A	E_A [kcal mol^{-1}K^{-1}]
1	$N_2 + O \leftrightarrow NO + N$	$7.6\times10^{13}/1.6\times10^{13}$	0/0	–38000/0
2	$O_2 + N \leftrightarrow NO + O$	$6.4\times10^{9}/1.5\times10^{9}$	0/0	–3150/–19500
3	$OH + N \leftrightarrow NO + H$	$4.1\times10^{13}/2\times10^{14}$	0/0	0/–23650

The NO generation rate is [33]:

$$\begin{cases} \dfrac{\mathrm{d[NO]}}{\mathrm{d}t} = \dfrac{2R_1(1-\alpha^2)}{\dfrac{1+\alpha R_1}{R_2+R_3}} \\ \alpha = \dfrac{\mathrm{[NO]}}{\mathrm{[NO]_e}} \end{cases} \tag{21}$$

The $[\,]_\mathrm{e}$ represents the concentration at equilibrium. The other constants in the equation are expressed as:

$$\begin{cases} R_1 = k_{+1}[\mathrm{N_2}]_\mathrm{e}[\mathrm{O}]_\mathrm{e} = k_{-1}[\mathrm{NO}]_\mathrm{e}[\mathrm{N}]_\mathrm{e} \\ R_2 = k_{+2}[\mathrm{O_2}]_\mathrm{e}[\mathrm{N}]_\mathrm{e} = k_{-2}[\mathrm{NO}]_\mathrm{e}[\mathrm{O}]_\mathrm{e} \\ R_3 = k_{+3}[\mathrm{OH}]_\mathrm{e}[\mathrm{N}]_\mathrm{e} = k_{-3}[\mathrm{NO}]_\mathrm{e}[\mathrm{H}]_\mathrm{e} \end{cases} \tag{22}$$

Model verification and Miller cycle cases

Model verification

All measurements of this engine are from the official workshop test report certified by CCS (China Classification Society) and LR (Lloyd's Register of Shipping). The basic parameters of the engine are shown in tab. 3.

Table 3. Specification of dual-fuel engine (100% load)

Engine parameters	Specifications
Cylinder number [–]	8
Cylinder diameter [mm]	510
Stroke [mm]	600
Compression ratio [–]	13.3
Power [kW]	8000
Speed [rpm]	514
Fire order [–]	1-4-7-6-8-5-2-3

Figure 2 shows the comparison between the calculated and the measured error under different loads. It can be seen that the error of all the main parameters is within 3%, and the fuel consumption and power error are within 1%, which indicate that the simulation model can meet the calculation requirements. Figure 3 shows the cylinder simulation pressure under different loads.

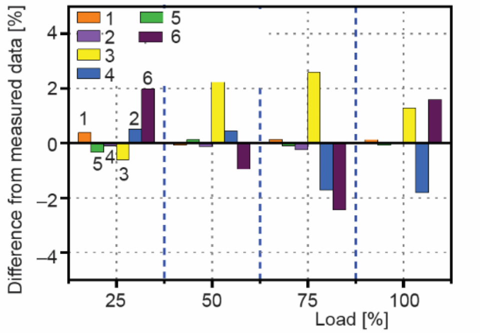

Figure 2. Comparison of model and measurement; *1 – power, 2 – intake manifold pressure, 3 – exhaust manifold pressure, 4 – peak pressure, 5 – BSFC, 6 – NO$_x$*

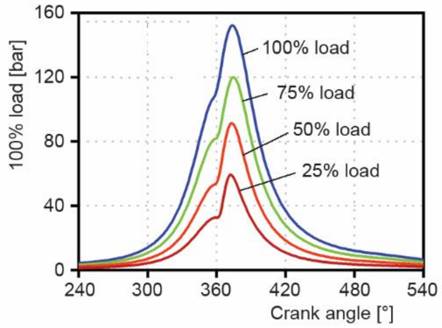

Figure 3. Comparison of cylinder pressure simulation

Considering the maximum NO$_x$ emission flow rate at 50% load, therefore, the Miller cycle is used to optimize the 50% load condition. Table 4 shows the error between the simulation and measure values at 50% load.

Table 4. Comparison of experimental main parameters with calculated one at 50% load

Main Parameters	Measured	Calculated	Error
Power [kW]	4004	4000	–0.10%
BSFC converted [gk^{-1}W^{-1}h^{-1}]	172.1	172.4	0.17%
Intake manifold temperature [K]	321	321.2	0.06%
Intake manifold pressure [bar]	111	112.6	1.44%
Intake manifold mass flow [kgs^{-1}]	6.91	6.92	0.14%
Exhaust manifold temperature [K]	789	789.7	0.09%
Exhaust manifold pressure [bar]	1.526	1.56	2.23%
NO$_x$ flow [kgh^{-1}]	18.77	18.51	–1.39%
Peak pressure [bar]	91	91.3	0.33%

Model cycle calculation cases

Compared with the LIVC Miller cycle, the EIVC Miller cycle pumping loss is lower, so the EIVC method is chosen in this paper to achieve the Miller cycle [21]. Figure 4 shows the comparison of different Miller cycle valve timing. The original valve closing time is 558 °CA (Base), and the EIVC Miller cycle are 520 °CA (M520), 510 °CA (M510), 500 °CA (M500), and 490 °CA (M490). To maintain the approximate intake air mass and temperature, two-stage turbocharger or more efficient turbocharger and more efficient intercooler or greater

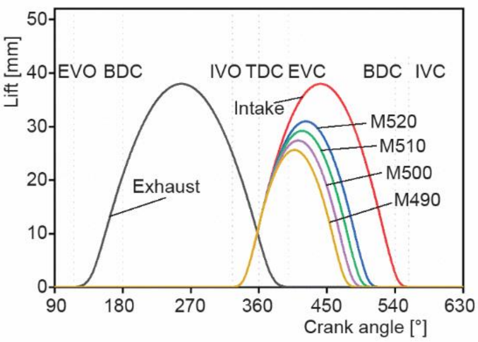

Figure 4. Valve lift curves

cooling water flow are needed in the actual test. However, it can directly improve the efficiency of the compressor and intercooler in the simulation research to meet the same intake mass-flow and temperature requirement, which will not affect the study of the Miller cycle.

Table 5 shows the initial conditions of the calculation. The intake air temperature remains the same due to the same load. The values in the table are the averages of the final simulation after stabilization. In all the cases, it is assumed that the temperature of the cylinder head, the cylinder wall and the piston crown are the same under different cases.

Table 5. The initial conditions in the calculation

50% load	Base	M520	M510	M500	M490
Intake Pressure [bar]	1.98	2.70	2.99	3.34	3.78
Intake temperature [K]	321.2	320.6	320.5	320.6	321.0
Exhaust pressure [bar]	1.56	2.05	2.26	2.51	2.83
Exhaust temperature [K]	789.7	795.3	800.3	807.1	817.9
Head temperature [K]	783				
Liner temperature [K]	723 at TDC and 623 at BDC				
Piston temperature [K]	873				

Results and discussion

Figure 5 shows the comparison of the intake pressure and the TDC. It can be seen from the figure, with the advance of IVC angle, the intake pressure increases. Since the intake valve is closed early, the in-cylinder charge expands and cools down. The effective compression stroke is shortened and the effective compression ratio is reduced. The temperature at TDC decreases with the earlier angle of the IVC, and the M490 calculation simulation is reduced by 136 K compared with the original engine. This conclusion is consistent with previous studies [34].

Figure 6 shows the comparison of power and fuel consumption. With the advance of IVC angle, the effective compression stroke becomes shorter. The lower effective working volumes results in lower thermal efficiency, higher fuel consumption and lower power.

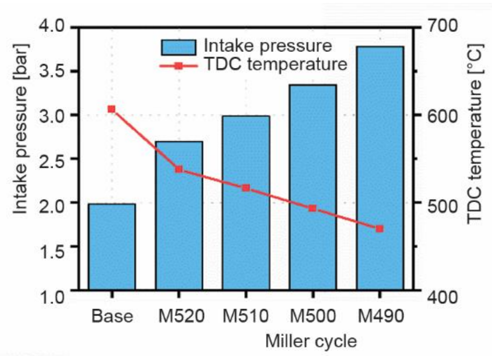

Figure 5. Comparison of intake pressure and TDC temperature

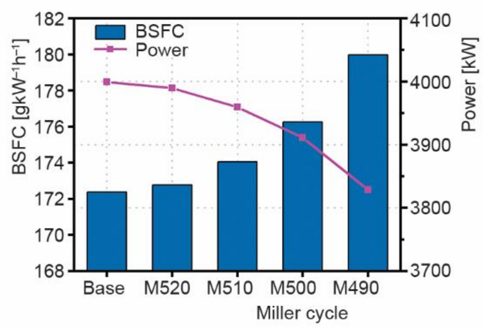

Figure 6. Comparison of power and fuel consumption

Figure 7 shows the comparison of NO_x emissions and exhaust manifold temperature. The NO_x emissions is affected by combustion temperature in cylinder. The cylinder charge expands and cools with the advance of IVC angle which leads to the lower effective compression ratio [35]. This causes the temperature of the entire combustion process to decrease, which greatly deteriorates the NO_x generation conditions and greatly reduces the NO_x emissions. The increase in the intake pressure causes the enthalpy of the charge in the cylinder to increase, resulting in an increase in the exhaust gas temperature.

Figure 8 shows the trend of pressure and heat release rate in the cylinder. With the advance of IVC angle, the intake pressure increases, which delays the start of combustion, increases the duration of combustion and moves the heat release center back. This coincides with previous works [21]. This causes the cylinder peak pressure to shift back and the peak pressure to drop, which reduces the geometric load on the engine and helps to improve the reliability of the engine.

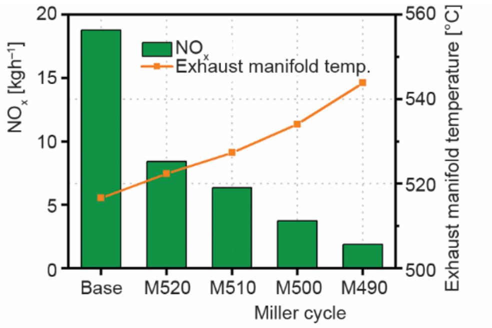

Figure 7. Comparison of NO_x emissions and exhaust manifold temperature

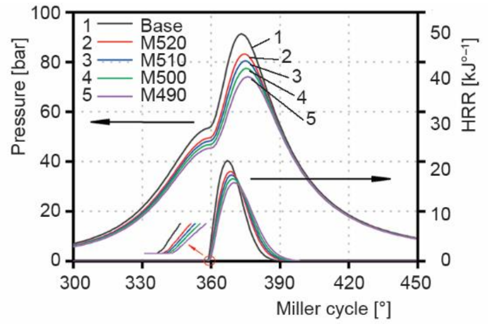

Figure 8. Comparison of cylinder pressure and heat release rate

Figure 9 shows the 3-D diagram of fuel consumption, compression ratio and NO_x emissions. With the advance of IVC angle, the effective compression ratio decreases, which leads to the lower thermal efficiency, higher fuel consumption and lower power consumption [36]. This problem can be effectively solved by increasing the geometric compression ratio. The geometric compression ratio and Miller cycle have opposite effects on engine NO_x emissions. The higher geometric compression ratio causes the higher cylinder maximum combustion temperature and increases the NO_x emissions. In all optimization cases, the fuel consumption of the M520-CR13.3, M510-CR14 and M500-CR15 cases are almost the same, but the NO_x emissions of M500-CR15 case is lower. For all the M490 calculation cases, the fuel consumption cannot be improved by increasing the geometric compression ratio, so the M490 cases is not recommended in actual conditions. Considering the affection of the geometric compression ratio on the Miller cycle, the M510-14 case is the best solution for economics and emissions.

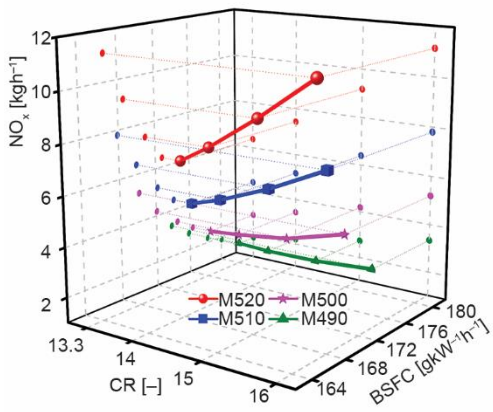

Figure 9. The 3-D plot of fuel consumption, compression ratio and NO_x emissions

Conclusions

The previous analyses show that the Miller cycle has a greater advantage in terms of emissions than the standard cycle. Compared with the original engine, in the M520 case, the NO_x emission is reduced by 65.5%, the fuel consumption is only increased by 0.24%, and the power is reduced by 0.27%. The earlier angle of the IVC can further reduce the NO_x emissions. In the M490 case, the NO_x emissions is reduced by 89%, but the combustion efficiency is also decreased. However, the Miller cycle increases the fuel consumption and reduces the power, in the original Miller cycle, the fuel consumption and power are improved by changing the compression ratio. In order to achieve less fuel consumption and higher power, the geometric compression is increased to the Miller cycle calculation cases. Considering NO_x emissions and fuel consumption, the NO_x emissions and fuel consumption are reduced by 72% and 0.1% respectively in the M510-CR14 case. In this paper, the early intake valve closing method of the Miller cycle is used to optimize the NO_x emissions. However, the earlier angle of the IVC needs higher intake pressure and requires a better turbocharger which limits the application of the Miller cycle. This paper provides a reasonable solution for dual-fuel engines operating on partial load and an important reference for reducing emissions optimization and meeting Tier III standards.

Acknowledgment

The research work has been financially supported by the People's Republic of China Project *Intelligent Ship Comprehensive Testing and Verification Research*, [2018] No. 473, also supported by *the Fundamental Research Funds for the Central Universities* (No. 3132019315). The authors also gratefully acknowledge the helpful comments and suggestions of the reviewers, which have improved the presentation.

Nomenclature

A – heat transfer area, [m^2]
B – bore, [m]
C_m – mean pistion velocity, [m s^{-1}]
c_p – constant pressure specific heat, [kJkg^{-1}K^{-1}]
c_v – constant volume specific heat, [kJkg^{-1}K^{-1}]
h – specific enthalpy, [kJkg^{-1}]
m – mass, [kg]
n – specific internal energy, [kJkg^{-1}]
p – pressure, [bar]
Q – heat loss, [kJkg^{-1}]
S – stroke, [m]
T – temperature, [K]
U – internal energy, [kJ]
V – volume, [m^3]
$\dot{W}$ – work output or input, [kJ]
w – pressure ratio, [–]
x – burn fraction, [–]

Greek symbols

ε – ratio of half stroke to rod length, [–]
ϕ – crank angle, [°]
γ – compression ratio index, [–]
η – efficiency, [–]

Subscripts

0 – start of combustion
1 – state at intake valve closing
a – ambient
b – burned zone
c – compressor
e – exhaust state
f – fuel (include diesel and natural gas)
i – intercooler
mot – engine motored
s – intake state
t – turbine
u – unburned zone
z – in cylinder state parameters
w – cylinder walls

Acronyms

BSFC – brake specific fuel consumption, [gK^{-1}W^{-1}h^{-1}]
CA – crank angle
HRR – heat release rate
IMEP – indicated mean effective pressure, [bar]
IVC – intake valve closing

References

[1] Guan, B., *et al.*, Review of State of the Art Technologies of Selective Catalytic Reduction of NOx from Diesel Engine Exhaust, *Applied Thermal Engineering, 66* (2014), 1, pp. 395-414

[2] Jeong, S.-J., *et al.*, Numerical Study on the Optimum Injection of Urea–Water Solution for SCR DeNOx System of a Heavy-Duty Diesel Engine to Improve DeNOx Performance and Reduce NH_3 Slip, *Environmental Engineering Science, 25* (2008), 7, pp. 1017-1036

[3] Pueschel, M., *et al.*, Combination of Post-Injection and Cooled EGR at a Medium-Speed Diesel Engine to Comply with IMO Tier III Emission Limits, *Proceedings*, CIMAC, Shanghai, 2013, pp. 76-84

[4] Scappin, F., *et al.*, Validation of a Zero-Dimensional Model for Prediction of NOx and Engine Performance for Electronically Controlled Marine Two-Stroke Diesel Engines, *Applied Thermal Engineering, 37* (2012), 1, pp. 344-352

[5] Zhou, S., *et al.*, Evaluation of Miller Cycle and fuel Injection Direction Strategies for Low NOx Emission in Marine Two-Stroke Engine, *International Journal of Hydrogen Energy, 42* (2017), 31, pp. 20351-20360

[6] Hegab, A., *et al.*, Towards Keeping Diesel Fuel Supply and Demand in Balance: Dual-fuelling of Diesel Engines With Natural Gas, *Renewable and Sustainable Energy Reviews, 70* (2017), 1, pp. 666-697

[7] Carlucci, A. P., *et al.*, Study of Combustion Development in Methane-Diesel Dual Fuel Engines, Based on the Analysis of In-Cylinder Luminance, *Proceedings*, SAE 2010 World Congress and Exhibition, Detroit, Mich., USA, 2010

[8] Carlucci, A. P., *et al.*, Combustion and Emissions Control in Diesel-Methane Dual Fuel Engines: The Effects of Methane Supply Method Combined with Variable In-Cylinder Charge Bulk Motion, *Energy Conversion and Management, 52* (2011), 8, pp. 3004-3017

[9] Li, W., *et al.*, Experimental and Theoretical Analysis of the Combustion Process at Low Loads of a Diesel Natural Gas Dual-Fuel Engine, *Energy, 94* (2016), Jan., pp. 728-741

[10] Li, W., *et al.*, Experimental and Theoretical Analysis of Effects of Equivalence Ratio on Mixture Properties, Combustion, Thermal Efficiency and Exhaust Emissions of a Pilot-Ignited NG Engine at Low Loads, *Fuel, 171* (2016), May, pp. 125-135

[11] Kesgin, U., Efficiency Improvement and NOx Emission Reduction Potentials of Two-Stage Turbocharged Miller Cycle for Stationary Natural Gas Engines, *International Journal of Energy Research, 29* (2005), 3, pp. 189-216

[12] Wang, Y., *et al.*, An analytic Study of Applying Miller Cycle to Reduce NOx Emission from Petrol Engine, *Applied Thermal Engineering, 27* (2007), 11, pp. 1779-1789

[13] Mikalsen, R., *et al.*, A Comparison of Miller and Otto Cycle Natural Gas Engines for Small Scale CHP Applications, *Applied Energy, 86* (2009), 6, pp. 922-927

[14] Gonca, G., Sahin, B., Effect of Turbo Charging and Steam Injection Methods on the Performance of a Miller Cycle Diesel Engine (MCDE), *Applied Thermal Engineering, 118* (2017), 1, pp. 138-146

[15] Tavakoli, S., *et al.*, Miller Cycle Application to Improve Lean Burn Gas Engine Performance, *Energy, 109* (2016), Aug., pp. 190-200

[16] Yan, B., *et al.*, The Effects of LIVC Miller Cycle on the Combustion Characteristics and Thermal Efficiency in a Stoichiometric Operation Natural Gas Engine with EGR, *Applied Thermal Engineering, 122* (2017), 1, pp. 439-450

[17] Kayadelen, H., *et al.*, Comparison of Diesel Engine and Miller Cycled Diesel Engine by Using Two Zone Combustion Model, *Proceedings*, 1st International Symposium on Naval Architecture and Maritime, Istanbul, Turkey, 2011

[18] Gonca, G., *et al.*, Comparison of Steam Injected Diesel Engine and Miller Cycled Diesel Engine by Using Two Zone Combustion Model, *Journal of the Energy Institute, 88* (2015), 1, pp. 43-52

[19] Provataris, S. A., *et al.*, Prediction of NOx Emissions for High Speed DI Diesel Engines Using a Semi-empirical, Two-Zone Model, *Energy Conversion and Management, 153* (2017), Dec., pp. 659-670

[20] Clarke, D., Smith, W. J., The Simulation, Implementation and Analysis of the Miller Cycle Using an Inlet Control Rotary Valve, SAE Tehnical Paper, 1997-02-24,1997

[21] Li, T., *et al.*, The Miller Cycle Effects on Improvement of Fuel Economy in a Highly Boosted, High Compression Ratio, Direct-Injection Gasoline Engine: EIVC *vs.* LIVC, *Energy Conversion and Management, 79* (2014), Mar., pp. 59-65

[22] Pedrozo, V. B., Zhao, H., Improvement in High Load Ethanol-Diesel Dual-Fuel Combustion by Miller Cycle and Charge Air Cooling, *Applied Energy, 210* (2018), 1, pp. 138-151

[23] Miller, R. H., Supercharging and Internal Cooling Cycle for High Output, *ASME Transactions, 69* (1947), pp. 453-457
[24] Lounici, M. S., *et al.*, Investigation on Heat Transfer Evaluation for a More Efficient Two-Zone Combustion Model in the Case of Natural Gas SI Engines, *Applied Thermal Engineering, 31* (2011), 2, pp. 319-328
[25] Ghojel, J., Review of the Development and Applications of the Wiebe Function: A Tribute to the Contribution of Ivan Wiebe to Engine Research, *International Journal of Engine Research, 11* (2010), 4, pp. 297-312
[26] Hires, S. D., *et al.*, The Prediction of Ignition Delay and Combustion Intervals for a Homogeneous Charge, Spark Ignition Engine, SAE Technical Paper, 1978-02-01, 1978
[27] Gu, X. J., *et al.*, Laminar Burning Velocity and Markstein Lengths of Methane-Air Mixtures, *Combustion and Flame, 121* (2000), 1, pp. 41-58
[28] Merker, G. P., *et al.*, *Simulating Combustion: Simulation of combustion and pollutant formation for engine-development*. Springer Science & Business Media, New York, USA, 2005
[29] Moran, M. J., *et al.*, *Fundamentals of engineering thermodynamics*, John Wiley & Sons, New York, USA, 2010
[30] Chang, J., *et al.*, New Heat Transfer Correlation for an HCCI Engine Derived from Measurements of Instantaneous Surface Heat Flux, *SAE Transactions, 113* (2004), 3, pp. 1576-1593
[31] Woschni, G., A Universally Applicable Equation for the Instantaneous Heat Transfer Coefficient in the Internal Combustion Engine, *SAE Transactions, 76* (1968), pp. 3065-3083
[32] Gonca, G., *et al.*, Theoretical and Experimental Investigation of the Miller Cycle Diesel Engine in Terms of Performance and Emission Parameters, *Applied Energy, 138* (2015), 1, pp. 11-20
[33] Tang, Y., *et al.*, Investigation on the Solution of Nitric Oxide Emission Model for Diesel Engine Using Optimization Algorithms, *Fuel, 228* (2018), 1, pp. 81-91
[34] Zhang, J., *et al.*, Effects of Early Intake Valve Closing on Characteristics of Cyclic Variations in Diesel Engine, *Transactions of Csice, 34* (2016), 5, pp. 401-408
[35] Benajes, J., *et al.*, Potential of Atkinson Cycle Combined with EGR for Pollutant Control in a HD Diesel Engine, *Energy Conversion and Management, 50* (2009), 1, pp. 174-183
[36] Zammit, J. P., *et al.*, The Effects of Early Inlet Valve Closing and Cylinder Disablement on Fuel Economy and Emissions of a Direct Injection Diesel Engine, *Energy, 79* (2015), Jan., pp. 100-110

Paper submitted: June 8, 2019
Paper revised: July 1, 2019
Paper accepted: July 4, 2019